HHS Public Access

Author manuscript

Free Radic Biol Med. Author manuscript; available in PMC 2020 December 18.

Published in final edited form as:

Free Radic Biol Med. 2020 April ; 150: 75–86. doi:10.1016/j.freeradbiomed.2020.02.010.

A low glycemic diet protects disease-prone Nrf2-deficient mice against age-related macular degeneration

Sheldon Rowan[1,2,3,*], **Shuhong Jiang**[1,4], **Min-Lee Chang**[1], **Jonathan Volkin**[1], **Christa Cassalman**[5], **Kelsey M. Smith**[1,2], **Matthew D. Streeter**[6], **David A. Spiegel**[6], **Carlos Moreira-Neto**[3], **Naila Rabbani**[7,8], **Paul J. Thornalley**[7,9], **Donald E. Smith**[1], **Nadia K. Waheed**[3], **Allen Taylor**[1,2,3,*]

[1]Laboratory for Nutrition and Vision Research, JM-USDA Human Nutrition Research Center on Aging, Tufts University, Boston, MA, 02111, USA

[2]Friedman School of Nutrition and Science Policy, Tufts University, Boston, MA, 02111, USA

[3]Department of Ophthalmology, Tufts University School of Medicine, Boston, MA, 02111, USA

[4]Inner Mongolia Autonomous Region People's Hospital, Hohhot, Inner Mongolia 010017, China

[5]Department of Pathology and Laboratory Medicine, Tufts University School of Medicine, Boston, MA 02111, USA

[6]Department of Chemistry, Yale University, New Haven, CT 06520, USA

[7]Clinical Sciences Research Laboratories, Warwick Medical School, University of Warwick, University Hospital, Coventry, CV2 2DX, UK

[8]Department of Basic Medical Sciences, College of Medicine, QU Health, Qatar University, P.O. Box 2713, Doha, Qatar.

[9]Diabetes Research Center, Qatar Biomedical Research Institute, Hamad Bin Khalifa University, Qatar Foundation, P.O. Box 34110, Doha, Qatar.

Abstract

Age-related macular degeneration (AMD) is a major blinding disease, affecting over 14% of the elderly. Risk for AMD is related to age, diet, environment, and genetics. Dietary modulation of AMD risk is a promising treatment modality, but requires appropriate animal models to demonstrate advantages of diet. Mice lacking the antioxidant transcription factor Nrf2 (*Nfe2l2*) develop age-related retinopathy relevant to human AMD. Here we evaluated the effect of consuming high glycemic (HG) or low glycemic (LG) diets until 18-months of age on development of features relevant to AMD in Nrf2-null mice. Nrf2-null mice that consumed HG diets developed atrophic AMD, characterized by photoreceptor degeneration, retinal pigment epithelium (RPE) atrophy and pigmentary abnormalities, basal laminar deposits, and loss of the choriocapillaris. In contrast, Nrf2-null-mice that consumed LG diets did not develop retinal disease phenotypes. Consumption of HG diets was associated with accumulation of advanced glycation end-products in the RPE and systemically, whereas consumption of the LG diet was

*Corresponding authors. allen.taylor@tufts.edu or sheldon.rowan@tufts.edu.

associated with increased levels of anti-glycative and anti-oxidative detoxification machinery. Together our data indicate that the Nrf2-null HG mouse is a good model for atrophic AMD studies and that the LG diet can activate protective pathways to prevent AMD, even in a genetically predisposed animal.

Keywords

advanced glycation end-product; geographic atrophy; retinal pigmented epithelium; glycemic index; antioxidant

Introduction

Age-related macular degeneration (AMD) is the leading cause of blindness in industrialized nations and prevalence of AMD is accelerating due to increasingly aging populations globally and a changing food environment. Advanced AMD can be neovascular (wet AMD), comprising approximately 15% of cases, or atrophic (dry AMD), accounting for the remaining 85% of cases. Whereas neovascular AMD can be treated using anti-angiogenic agents, there is no current treatment for advanced atrophic AMD, in which the retinal pigmented epithelium (RPE) degenerates, associated with loss of photoreceptor cells and visual dysfunction. Often, diagnosis only follows some loss of vision, making prevention challenging. A dearth of biochemical biomarkers for early AMD compounds this frustration, although decrements in retinal function have been documented (1).

Progression of intermediate to advanced AMD can be slowed in some patients via the AREDS2 supplements containing high doses of vitamin C, vitamin E, zinc, lutein, and zeaxanthin (2). Epidemiological evidence supports the notion that a healthy diet can prevent early AMD and progression to advanced AMD (3–5). In particular, consumption of healthy dietary patterns like the Mediterranean diet or low glycemic index diets seem to protect against AMD (5–11), whereas consumption of a Western dietary pattern or high glycemic index diets appear to increase risk for AMD (7, 12–14). Many of these findings have been corroborated experimentally in disease model systems, notably in mouse and primate models (15–18).

Understanding more about the etiology of AMD would inform about ways to delay onset or progress of the disease. Pathomechanistic investigations of AMD have been enhanced by the use of genetic and cellular model disease systems. Studies in mice and human RPE cells have shown that oxidative damage, lipid accumulation, mitochondrial dysfunction, inflammatory damage, and loss of protein quality control all are associated with AMD pathogenesis (19–24). Many of these mechanisms are recapitulated by dietary stress. Wildtype mice fed a high glycemic (HG) diet and aged to 24-months develop features of AMD, which can be arrested, and possibly even reversed, by dietary change to a low glycemic (LG) diet (18). We proposed that among mechanisms behind the HG diet-AMD connection is glycation-induced modification of bulk proteins, including accumulation of advanced glycation end-products (AGEs) in the eye (17, 18, 25). AGEs are formed by non-enzymatic reaction of sugars or their catabolites with proteins and other biomolecules compounded by oxidative and other stresses. Collectively these modifications are known as

glycation. AGEs are cytotoxic and have been shown to be increased locally and systemically in AMD (26–30). Accumulation of AGEs compounds cellular vulnerability by impairing protein quality control processes that remove aggregated and damaged protein and lipid species (25, 31). Formation of AGEs can be limited by either reducing glycemia or by reducing oxidative stress; both mechanisms also appear to reduce risk for AMD (2, 32).

Nrf2 is a transcription factor that targets and upregulates key antioxidant systems including glutathione and thioredoxin, phase I and phase II detoxification machinery, NADPH regeneration, heme and iron metabolism (33). Nrf2 also activates glyoxalase I (Glo1), which detoxifies precursors of AGEs, including methylglyoxal, the major glycating product of glucose catabolism, thus preventing AGE formation (34–37). Nrf2 itself is glycated, leading to diminution of its antioxidant function (38). Additionally, Nrf2 helps to regulate metabolic and autophagic pathways, which together preserve protein quality control and cellular health (39, 40). These functions are, in part, via the role of Nrf2 in maintenance of mitochondrial biogenesis, distribution, and function (40–42). Nrf2 regulates mitochondrial biogenesis in concert with PGC-1α, a critical transcriptional regulator of mitochondrial biogenesis (43). Consistent with these diverse cellular functions, loss of Nrf2 in mice damages many organs systems, such as the liver, lung, and brain, and predisposes mice to several neoplasias (44–48).

In the eye, loss of Nrf2 renders mice susceptible to vascular damage caused by ischemia-reperfusion injury (49). The eyes of Nrf2-deficient animals show signs of retinopathy, including AMD features, between 12–16 mo. of age (50, 51). In response to a high-fat diet, Nrf2-null mice develop more extensive RPE degeneration, characterized by subretinal drusenoid deposits that progress in size and number (51). The AMD-like phenotypes are further worsened by combined loss of Nrf2 and PGC1α. Together these suggest that mitochondrial damage and reactive oxygen species generation caused by PGC1α deficiency, coupled with an impaired antioxidant response caused by Nrf2 deficiency, leads to AMD pathogenesis (52). Conversely, overexpression of Nrf2 can rescue retinal degeneration in an inherited model of retinitis pigmentosa (53). Nrf2 can also be activated by other cytoprotective pathways, such as the sigma1 receptor chaperone, to rescue cone photoreceptor degeneration (54). In response to high-fat dietary stress, cigarette smoke, exogenous oxidative stress, and aging, Nrf2 function declines, contributing to RPE degenerative processes (55, 56), resembling those occurring in geographic atrophy, a late form of dry AMD. Nrf2 is thus related to AMD etiology through the increase in oxidative damage in the RPE during normal aging, functional decline of Nrf2 transcriptional responses in the RPE during aging, and transcriptionally-independent functions of Nrf2 in maintenance of mitochondrial quality control (57).

Here we sought to understand the interaction of diet-induced glycemia, as elicited by the same amount of less or more readily digested carbohydrate, on age-related retinal health within the context of Nrf2 deficiency. Specifically, we tested the hypothesis that feeding Nrf2-null mice an HG diet would induce glycemic and glycative stresses that would lead to progressive eye pathology. Conversely, we expected that the LG diet would promote health in both wildtype and Nrf2-null mice. We found that Nrf2-null mice fed HG diets developed atrophic AMD-like disease, but Nrf2-null mice fed LG diets were protected from

retinopathy at 18-months of age. Therefore, Nrf2-null mice fed an HG diet represent a new accelerated model relevant to dry AMD, and the LG diet represents a potential therapeutic intervention to limit risk or progress of AMD.

Results

In order to test whether diet can modulate ocular phenotypes in Nrf2-null mice, we fed male Nrf2-null mice calorically matched HG or LG diets, beginning at 12-weeks of life (simplified hereon as Nrf2-HG or Nrf2-LG). Food consumption was monitored and mice in HG or LG groups were fed the same amount of food such that both groups consumed equal amounts of diets. They were killed at 18-months. Nrf2-HG mice gained weight and became obese, comparable to wildtype mice fed HG diets (WT-HG) (18, 58, 59), but different from Nrf2-null mice that are generally resistant to obesity when fed high-fat diets (60). In comparison, Nrf2-LG mice, like wildtype mice fed LG diets (WT-LG), remained lean throughout the study (Fig. 1A,B). The difference in weights was due to increased fat mass in the Nrf2-HG mice (Fig. 1B). Along with increased fat mass, Nrf2-HG mice were hyperglycemic and glucose intolerant, while Nrf2-LG mice maintained normal glycemia (Fig. 1C,D). Nrf2-HG mice had increased levels of fasting plasma insulin, indicating that they were insulin resistant (Fig. 1E).

In order to assess effects of elevated glycemia on retinal health of Nrf2-null mice fed HG or LG diets, we performed histological analysis of retinas from 18-month old mice. First, we compared Nrf2-null mice fed HG or LG diets to WT mice fed identical diets. WT-LG or Nrf2-LG mice had intact, normally laminated retinas and a typical monolayered RPE (Fig. 2A,B, S1A,B). 18-month WT-HG mice also had grossly normal retinal lamination and structure (Fig. 2C, S1C), although quantitative studies did reveal mild thinning of the ONL (Fig. 2I). In comparison, Nrf2-HG mice presented with many retinal abnormalities, including a dramatic thinning of the ONL (Fig. 2D–F, 2I) and atrophy of the RPE (Fig. 2D–F, S1D-F). RPE atrophy was observed both localized (Fig. 2D, 2F, S1D, S1F) or more broadly (Fig. 2E, S1E) and was often associated with more dramatically thinned ONL. Some Nrf2-HG retinas developed large lesions that displaced the RPE and overlying photoreceptors (Fig. 2F, S1F). We also observed detachment of the RPE from Bruch's membrane (Fig. 2G,H, S1G,H), hypopigmentation of the RPE (Fig. 2H, S1H) and dysmorphia of the RPE (Fig. 2H) in Nrf2-HG retinas. Together, the retinal phenotypes observed in Nrf2-HG mice resemble those seen in dry AMD in humans, particularly RPE atrophy, photoreceptor loss, pigmentary changes, deposits, and RPE dysmorphia (61–63).

In order to better quantify phenotypic changes and variance, we quantified ONL thickness across the whole retina in 18-month WT and Nrf2-null mice fed HG or LG diets (Fig. 2I). In both genotypes, HG-fed mice had thinner ONLs than LG-fed mice, and Nrf2-null mice had thinner ONLs than WT mice. To more easily relate ONL thinning to other parameters, we computed a retinal damage score, calculated as the inverse of the area under the ONL thickness curve and scaled so that 24-month WT LG-fed mice had a score of 0, as we did previously (Fig. 2J and (18)). A retinal damage score less than 0 indicates a thicker ONL than 24-month WT LG-fed mice, typically observed in younger mice (18). Hence, larger positive values indicate worse scores. Consistent with the crucial protective role of Nrf2,

both diet groups of Nrf2−/− mice had higher retinal damage scores than WT-LG mice (Fig. 2J). Nrf2-HG mice had retina damage scores that were significantly higher than WT-HG mice ($P=1.2\times10^{-5}$) and Nrf2-LG mice ($P=1.4\times10^{-6}$) (Fig. 2J). Strikingly, Nrf2-LG mice had retinal damage scores similar to those observed in WT-HG mice. On average 18-month Nrf2-HG retina damage scores were higher than 24-month WT-HG-fed mice (11.8 +/− 3.3 for Nrf2-HG and 6.4 +/− 3.9 for WT-HG (Fig. 2J and (18))). Using a general linear model, we found that diet and genotype were each significantly associated with retinal damage score (diet: $P=3.7\times10^{-9}$; genotype: $P=8.1\times10^{-8}$), but there was no gene-diet interaction (P=0.56).

Another indicator of AMD in humans is pigmentary abnormalities, both hyper and hypopigmentation, which may be related to earlier RPE changes. We found that Nrf2-HG mice had broad areas of hypopigmentation as well as hyperpigmentation, whereas Nrf2-LG mice had more typical fundus appearances of 18-mo. mice (Fig. 3A–D). Histological analysis of the RPE revealed overall quantitative hypopigmentation of Nrf2-HG RPE (Fig. 3E–H), as well as RPE thinning and atrophy (Fig. 3E,F, I, J). We observed a linear relationship between RPE hypopigmentation or RPE thinning and retina damage score (Fig. 3H, J), consistent with the relationship between RPE and photoreceptor degeneration that is seen in atrophic AMD in people.

Several additional hallmarks of AMD were visualized in electron micrographs (EM) of 18-mo. RPE. Nrf2-LG RPE often showed several large spindle-shaped pigment granules (melanosomes) and intact mitochondria overlying the basal infoldings, similar to the appearance of WT LG-fed mice (Fig. 4A, Supplementary Fig. 2) and healthy younger mice (64). In contrast, Nrf2-HG RPE had many disease features usually observed in mouse AMD models, including large basal laminar deposits (Fig. 4B), accumulation of lipofuscin granules (Fig. 4B, 4C, 4I), and loss or displacement of basal infoldings. Incidences of hyperpigmentation and hypopigmentation seen in fundus imaging and histology were also evident at the cellular level (Fig. 4D–E). We also observed severe mitochondrial degeneration in Nrf2-HG RPE, as indicated by vacuolated and swollen mitochondria (Fig. 4C–E). Finally, we occasionally observed infiltrating cells, likely monocytes/macrophages, between the RPE plasma membrane and Bruch's membrane (Fig. 4F). Recruitment of macrophages to Bruch's membrane has been observed in human AMD, sometimes in association with lipid-filled debris (65).

In order to corroborate the findings above, we quantified cytosolic area and numbers of lipofuscin granules from Nrf2-null LG or Nrf2-null HG RPE EM images. As might be expected if cellular area is displaced by deposits or vacuoles, cytoplasmic area was quantitatively smaller in Nrf2-null HG RPE than Nrf2-LG RPE (Fig. 4G), and negatively associated with retina damage score (Fig. 4H). Lipofuscin granules were increased in Nrf2-null HG RPE (Fig. 4I), and positively associated with retina damage score (Fig. 4J). Increased lipofuscin granules and decreased cytoplasmic area was also observed in 18-mo. RPE from WT HG-fed (Supplementary Fig. 2C,D).

We also evaluated Bruch's membrane and the choriocapillaris. Nrf2-LG RPE had a normal pentalaminar Bruch's membrane and well-defined fenestrated choriocapillaris (Fig. 5A,

S3A-C) whereas Nrf2-HG RPE was associated with basal deposits, including outer collagenous layer deposits (Fig. 5B–C), irregular and possibly lipid-filled deposits within Bruch's membrane (Fig. 5D–F), and other irregular deposits or debris within Bruch's membrane (arrow, Fig. 5B). We also observed frequent loss of the choriocapillaris and larger choroidal blood vessels in the Nrf2-HG eyes (Fig. 5B, 5D–F, S3D-F), in some cases leading to the direct juxtaposition of the normally distally located choroidal melanocytes directly against Bruch's membrane (Fig. 5F, S3D). When present, the choriocapillaris was constricted down the diameter of a red blood cell, had lost endothelial cell fenestrations, and sometimes contained macrophages, a finding observed in AMD (66) (Fig. S3D-F). We confirmed our EM-based analyses in sections from Nrf2-LG or Nrf2-HG eyes using Isolectin B4 to label blood vessels or autofluorescence as a surrogate for lipofuscin levels (Fig. 5G–J). Nrf2-LG eyes showed intact choriocapillaris, large choroidal blood vessels, and minimal autofluorescence, whereas Nrf2-HG eyes exhibited large regions devoid of the choriocapillaris and choroidal blood vessels, as well as increased and punctate autofluorescence within the RPE (Fig. 5I, J).

Taken together, our histological and ultrastructural characterizations of Nrf2-null eyes indicate that Nrf2-HG mice develop multiple, sometimes advanced, features of atrophic AMD, particularly RPE atrophy and loss of the choriocapillaris, while Nrf2-LG mice do not develop notable AMD phenotypes.

Next we explored a molecular basis for the diet-induced phenotypic differences between Nrf2-LG and Nrf2-HG animals. Nrf2 functions as an anti-glycation factor through activation of anti-oxidant pathways and by activating Glo1, the enzyme that is responsible for detoxifying the major glucose-derived metabolite and glycation agent, methylglyoxal. Consistent with these ascribed functions, Nrf2-null mice had twice the concentration of a major plasma AGE, MG-H1, than WT mice (Fig. 6A).

Within Nrf2-null mice, Nrf2-HG mice had increased plasma concentrations of pentosidine, a cross-linking AGE, and fructosyl-lysine, an early AGE product, compared with Nrf2-LG mice (Fig. 6B,C), consistent with the elevated glycemia observed in Nrf2-HG mice.

We also assessed AGE accumulation in the retina. Two different types of AGEs, Nω-(carboxyethyl)arginine (CEA), derived from methylglyoxal, and glucosepane, a cross-linking AGE, were both markedly increased in the RPE and choroid of Nrf2-HG mice, compared to Nrf2-LG mice (Fig. 6D–H). Differences in levels of AGEs were not clearly observed within the neural retina. Taken together, these data support the hypothesis that that Nrf2-LG RPE possesses increased capacity to detoxify or proteolytically remove AGEs relative to Nrf2-HG RPE.

We hypothesized that antioxidant and antiglycative enzymes, even those that are direct transcription targets of Nrf2, may be upregulated in Nrf2-LG RPE. To test this hypothesis, we evaluated the levels of three different enzymes that are targets of Nrf2 but may also be regulated in Nrf2-independent pathways. Copper-Zinc Superoxide Dismutase 1 (SOD1) mitigates oxidative stress, Glo1 limits formation of methylglyoxal, and Glutamate-Cysteine Ligase Modifier Subunit (GCLM) regulates synthesis of the major biological antioxidant

glutathione. All three proteins showed modestly increased levels in the RPE of Nrf2-LG mice compared with the Nrf2-HG (Fig. 7A–G).

Discussion

Given the dire need to combat the growing epidemic of AMD, it is crucial to develop treatments for AMD. This is particularly true for dry (atrophic) AMD, for which there are no remedies currently available. Our data establish Nrf2-HG mice as a new and potentially valuable model for atrophic AMD, and suggest a dietary intervention to delay AMD phenotypes. Compared with WT-HG mice, which develop AMD phenotypes at 24-months, Nrf2-HG mice show more severe phenotypes that are obvious at 18-months. Many of these lesions approximate those of advanced dry AMD, such as loss of the choriocapillaris and photoreceptors, mitochondrial degeneration, and basal deposits. We also demonstrate the ability to limit these phenotypes via intake of an LG diet. The LG diet exploited here is attractive in that it is comparable to human diets that are rich in whole grains and high in fiber, which have been shown to protect from AMD (6–10). Our data can be compared to other gene-diet studies that modulated AMD outcomes using different levels of dietary fats, cholesterol, or protective gene variants compared to AMD-associated gene variants (19, 67–70).

The Nrf2-HG model may also be useful for evaluating the role of the outer retinal vasculature in AMD. Imaging studies in human AMD have suggested that impaired choroidal blood flow precedes geographic atrophy (71). Furthermore, choriocapillaris degeneration is becoming better appreciated as a critical component of AMD and its progression to geographic atrophy (72). The RPE thinning and sub-RPE deposits, Bruch's membrane abnormalities, and loss of choriocapillaris in Nrf2-HG eyes suggest that the Nrf2-HG model should be useful for exploring the involvement of these tissues and the outer retinal vasculature in AMD and for testing drugs to preserve function of these tissues and cells. As with Nrf2-null high-fat diet-fed mice these Nrf2-HG mice had accelerated RPE degeneration and choroidal abnormalities but we did not observe significant subretinal drusen deposits and cell infiltration (51). Longitudinal imaging studies, coupled with tissue-specific knockouts of Nrf2, could further pathomechanistic understanding.

Our observation of ultrastructural changes and apparent mitochondrial degeneration in Nrf2-HG RPE (Fig. 4) indicate that the Nrf2-HG mouse may also be a useful model to study the role of mitochondrial dysfunction in AMD. This is of growing interest since mitochondrial degeneration has been directly or indirectly connected to human AMD (73–76). Experiments that directly target mitochondrial function in the RPE, such as *in vivo* delivery of PGC1α or pharmaceutical mimetics (77), may help elucidate the role of mitochondria in this AMD model.

What might be biochemical mechanisms by which the HG diet imparts damage to the retina? The accumulation of cytotoxic AGEs in the RPE of Nrf2-HG mice may be a critical pathogenic step explaining the observed RPE atrophy. Several different models could explain the AGE accumulation. A general explanation is that AGEs accumulate in Nrf2-HG mice due the chronic hyperglycemia, leading to higher levels of AGE precursors in

circulation. This hypothesis is supported by findings of higher levels of the AGE precursor fructosyl-lysine in the plasma and CEA/MG-H3 in the RPE of Nrf2-HG mice compared with Nrf2-LG mice (Fig. 6,7). However, other AGEs including MG-H1 were not increased in the plasma of Nrf2-HG mice.

Another model invokes protective machineries, i.e. that Nrf2-LG RPE has enhanced machinery to detoxify AGE precursors or proteolytically remove AGEs. In addition to the data indicated above and prior precedent, this model is supported by the finding of higher levels of Glo1, SOD1, and GCLM in the Nrf2-LG RPE (Fig. 7). Data from our group and others suggests that activation of protein quality control pathways like autophagy and the ubiquitin proteolysis system may facilitate removal of AGEs (25, 78–80). A corollary of this hypothesis is that upon aging and glycative stress, protective machineries are rendered less functional and/or insufficient to process the debris load that they encounter. Thus, damages and loss of function accrue at increasing rates. With limited antioxidant potential in a chronic high glycemic stress environment, the Nrf2-HG mouse typifies this, presenting features of AMD 6-months earlier than WT mice under the same conditions. The fact that we see differences in antioxidant enzymes and AGEs primarily in the RPE, corroborates decades of research indicating that the RPE is the processing site for retinal debris. Understanding the mechanisms of AGE formation and clearance in the RPE may reveal novel targets for AMD.

As the relationship between an LG diet and health in Nrf2-null mice appears similar to that seen in WT mice, there appear to be Nrf2-independent protective beneficial mechanisms that are reaped when consuming the LG diet. Metabolism is impacted by Nrf2 status and diet (81). Mice fed LG diets have higher levels of citric acid cycle intermediates like alpha ketoglutarate, fumarate, and malate, suggesting that the LG diet may promote oxidative phosphorylation over glycolysis (18). In order to spare energy for photoreceptors, RPE and photoreceptors use different sources of energy. Photoreceptors access glucose for survival, while RPE cells largely rely on lactate for oxidative phosphorylation (82). Dysregulated metabolism in the RPE, for instance via activation of the mTORC1 pathway, leads to RPE degeneration (83). RPE cells from AMD patients show altered bioenergetics, in particular reduced mitochondrial and glycolytic functions (76). This model is supported by the observation of improved RPE mitochondrial metabolism upon activation of AMPK signaling via metformin (84). The LG diet, therefore, may mirror metformin treatment to reduce glycemia and activate AMPK signaling.

Another mechanistic possibility is that the diet may indirectly affect AMD outcomes via the microbiome and gut health. The LG diet is known to affect the composition of gut microbiota (18). The gut microbial ecosystem is associated with, and may lead to reduced systemic inflammation (85), an established contributor to AMD pathogenesis (86–88). Patients with AMD have a significantly different gut microbiome than healthy controls (89). Nrf2-null mice have impaired gut barrier function, leading to bacterial endotoxin translocation across the gut (90). Hyperglycemic mice have similar phenotypes (91). Thus LG diet may enhance gut barrier function via effects on both microbiota composition and restoration of glycemic control.

Natural compounds that can activate the Nrf2 pathway, including the microbial metabolite urolithin A, derived from polyphenol-rich berries, or sulforaphane, a derivative of glucoraphanin that is found at high levels in cruciferous vegetables, similarly improve gut barrier function (92, 93). Direct injection of sulforaphane into the blood of mice or dietary consumption of glucoraphanin-rich broccoli sprout extract has been shown to improve metabolism and protect against diabetes (94). Therefore, pathways that can exploit Nrf2 or its functionality represent promising interventional targets to treat disease, particularly age-related diseases, where function of Nrf2 diminishes with age and oxidative stresses increase (21, 56).

Our work also expands knowledge about Nrf2-dependent functions in the eye and elsewhere. For example, the loss of photoreceptors cells in Nrf2-LG mice beyond what is observed in 18-month WT-LG mice (Fig. 2) or 24-month WT-LG mice (18), indicates diet-independent functions of Nrf2 in the eye. Similarly, Nrf2-HG mice developed AMD phenotypes beyond what is observed in WT-HG mice. Other diet-independent Nrf2-dependent phenotypes include liver cirrhosis and hepatocellular carcinoma (see Methods). We also defined diet-related phenotypes that were Nrf2-independent. These include effects of the HG diet on body weight and glucose tolerance (Fig. 1). Nrf2-null mice have impaired glucose tolerance when fed regular chow, due to a decreased islet volume and decreased hepatic expression of ChREBP, associated with decreased lipogenesis (95). Improvements of glycemia in Nrf2-LG mice may target the pancreas or the liver. The development of obesity and insulin resistance in Nrf2-null HG mice is somewhat surprising, since Nrf2-null mice have been reported to be resistant to diet-induced obesity (60). HG-induced obesity is preceded by impaired fat oxidation, which leads to elevated lipogenesis in the liver, increased insulin secretion, and further obesity (59, 96), a mechanism that is Nrf2-independent. The combination of Nrf2-independent and diet-independent functions in this animal model explains in part the lack of a clear gene-diet interaction and suggests benefits for optimizing both diet and enhancement of Nrf2 function in human populations.

In summary, our work indicates that the Nrf2-HG mouse is a new, accelerated model of atrophic AMD that provides opportunities to define critical pathogenic mechanisms for AMD development and timing windows for pharmaceutical or nutritional interventions. We describe one particularly promising intervention, the LG diet. Nrf2-LG mice had enhanced detoxification machinery in their RPE and were resistant to retinopathy described in Nrf2-null mice fed either regular diets or HG diets. The data presented also corroborate a significant body of prior laboratory investigation and human epidemiologic data that indicate that favoring LG carbohydrates over HG carbohydrates in the diet may provide an achievable, low-cost way to prolong retina function. That consuming low LG diets can limit the earliest indicators of AMD suggests that similar diets can be useful to delay loss of vision coincident with AMD. Optimizing Nrf2 or its functionality represent additional promising targets to treat age-related diseases, where function of Nrf2 diminishes with age and oxidative stresses increase (21, 56).

Materials and Methods

Animals and diets:

Nrf2 +/− and Nrf2 −/− mice (allele: *Nfe2l2*^{tm1Ywk}), maintained for at least 10 generations on a C57BL/6J genetic background, were obtained from Michael Freeman (Vanderbilt University) and Jackson Laboratories (Bar Harbor, ME) respectively, and were interbred to generate Nrf2 −/− mice.

Animals were fed standard chow ad libitum (Teklad 7012, Harlan Laboratories, Madison, WI) until 3-months of age, at which time they were placed on study diet. Thirty-nine Nrf2 −/− male mice were randomized into groups of 20 HG-fed mice and 19 LG-fed mice. Diets contained identical macronutrient compositions with the exception that the HG starch was composed of 100% amylopectin (Amioca starch, Ingredion Inc., Bridgewater, NJ), while the LG starch was composed of 70% amylose/30% amylopectin (Hylon VII starch, Ingredion Inc., Bridgewater, NJ)(17). Diet composition was 542 g/kg starch, 200 g/kg casein, 85 g/kg sucrose, 56 g/kg soybean oil, 50 g/kg wheat bran, 2 g/kg DL methionine, 10 g/kg vitamin mix, and 35 g/kg mineral mix. Macronutrient energy percentages were 65% carbohydrate, 21% protein, and 14% fat for both HG and LG diets. All diets were formulated by Bio-Serv (Frenchtown, NJ). Mice were group pair-fed to ensure equal consumption between diet groups.

Body composition analysis was performed at 13-months using an EchoMRI-700 to measure fat mass and lean body mass. At 18-months of age, mice were anesthetized with ketamine and xylazine, the fundus was photographed using a Micron III retinal microscope (Phoenix research labs, Pleasanton, CA), and fluorescein angiography images were acquired following intraperitoneal injection of fluorescein (Acorn). Mice were fasted for 6 hours and were subsequently killed. All animal work was performed at the Tufts University HNRCA and approved by the Tufts University IACUC in adherence with the ARVO statement for the use of animals in ophthalmic and vision research. Animals deemed to be in poor health were euthanized and excluded from the analysis. In total, 16 Nrf2-null HG mice (Nrf2-HG) and 17 Nrf2-null LG mice (Nrf2-LG) were included in the final analysis. 5 Nrf2-HG and 4 Nrf2-LG mice were found to have liver tumors upon necropsy.

Intraperitoneal glucose tolerance test and Insulin measurement:

Intraperitoneal glucose tolerance tests (IPGTT) were performed at 10-months. Mice were fasted for 6 h before IPGTT. A clean razor blade was used to make a horizontal cut in the lateral tail vein, releasing about 5 μl of blood that was applied to a OneTouch® Ultra® test strip in a OneTouch® Ultra2® glucometer (Lifescan Inc., Milpitas, CA) to obtain fasting glucose levels. For the glucose tolerance test, each mouse was injected intraperitoneally with 1 g/kg body weight D-(+)-glucose (≥99.5%, Sigma, St. Louis, MO) via a #25–5/8 gauge syringe. At 15, 30, 60 and 120 min after injection, repeated blood glucose measurements were performed as with the first measurement.

Insulin was measured at 18-months from fasted plasma samples, taken immediately prior to killing the mice, using the ultrasensitive mouse insulin ELISA kit, according to the manufacturer's instructions (Crystal Chem, Elk Grove Village, IL)

Transmission Electron Microscopy (EM) and Light Microscopy Analysis:

Eyes were removed and immediately fixed in EM fixative (2.5% glutaraldehyde, 2% paraformaldehyde, with 0.025% (w/v) CaCl2 in 0.1M sodium cacodylate buffer, pH 7.4). Eyes were washed 2 × 10 min in 0.1M sodium cacodylate buffer containing 5% sucrose, post-fixed 3.5 h in 1% osmium tetroxide in 0.1M cacodylate buffer containing 2% sucrose, washed 1 × 10 min in buffer and 1 × 10 min in distilled water (DW), and held in 4% uranyl acetate 1 h in the dark. Samples were then washed 1 × 10 min in DW, dehydrated 2 × 15 min each in graded ethanols (30%−100%) and propylene oxide, infiltrated in Embed-812 resin (Electron Microscopy Sciences, Hatfield, PA) for 24 on a rotator, and polymerized at 70 °C for 48 h. Sectioning was performed on a Leica EM UC7 Ultracut microtome using diamond knives (Diatome, Hatfield, PA). Semi-thin (0.5 μm) sections were stained with 1% toluidine blue in 1% sodium borate. Thin (silver) sections were collected on copper 135 hex grids, post-stained with 4% uranyl acetate in 50% (aq.) methanol and Reynold's lead citrate, and then viewed and photographed using a JEOL 1200 transmission electron microscope. Sections were photographed at 1mm from the optic nerve head. For semi-quantitative analysis of EM features, 35 20000X images were evaluated from 8–9 different eyes per group and parameters were then summarized per 100 μm of linear Bruch's membrane.

For light microscopy, semi-thin toluidine blue stained sections were photographed on an Olympus BX51 photomicroscope equipped with a DP70 digital camera with 24-bit depth. For morphometric analysis of RPE, 60x magnification images (dry objective, NA=0.8) were taken from independent sections of each eye. Images were taken approximately 1 mm from the optic nerve head, on the same side as where TEM images were photographed. Quantification was performed using ImageJ software (NIH), setting thresholds for pigmentation based on the red channel. Each section had a contiguous RPE stretch of 291 μm. For quantification of the outer nuclear layer, measurements were taken every 250 μm from the optic nerve head on superior and inferior hemispheres. These were averaged from two independent sections of each eye; 10–11 different eyes per group. High-magnification 100x images (Figure 3E–F, Supplementary Figure 1) were taken with an oil objective (NA=1.3).

Immunofluorescence and immunohistochemistry:

Enucleated eyes were immediately fixed in 4% paraformaldehyde for 1 hr. at 4 °C and transferred to PBS. The cornea and lens were removed, and the remaining eye cup was transferred to 30% sucrose for cryopreservation and then embedded in OCT. Cryosections were obtained at a thickness of 12 μm, dried overnight, and stored at −80°C.

For immunofluorescence, tissue sections were rehydrated in PBS containing 0.1% (v/v) Triton X-100 (PBT). For immunofluorescent detection of the RPE, slides were bleached using 10% hydrogen peroxide for 2 hrs. at 65°C. Next slides were blocked using normal donkey serum (Jackson Immunoresearch), incubated with primary antibodies for 2 hrs., washed with PBT, and incubated with appropriate secondary antibodies conjugated to either Cy3 or Alexa Fluor 488 (Jackson Immunoresearch). Slides were mounted in Prolong Gold Antifade with DAPI (Molecular Probes) and photographed on a Zeiss Axiovert fluorescence microscope and digital camera.

Primary antibodies and dilution:

Species	ID	Dilution	Source
Mouse	Anti-Nω-(carboxyethyl) arginine (CEA)	1:250	Ryoji Nagai
Rabbit	Anti-Glucosepane	1:200	David Spiegel
Rabbit	Anti-Superoxide dismutase 1 (SOD1)	1:500	Sigma
Rabbit	Anti-GCLM (Glutamate-Cysteine Ligase Modifier Subunit)	1:500	Abcam
Rabbit	Anti-Glo1	1:2000	Casper Schalkwijk (36)

Isolectin B4 staining was performed by incubating sections with Biotinylated Griffonia Simplicifolia Lectin I isolectin B4 (Vector Laboratories) followed by detection using Alexa Fluor 488-conjugated streptavidin (Invitrogen).

Statistical Analyses:

For univariate analyses, data were evaluated using either SPSS (IBM) or Microsoft Excel. First, data was evaluated as to whether it fit in a normal distribution or not, based on kurtosis and skewness. Pair-wise data that fit in a normal distribution was analyzed by a 2-tailed Student's t-test followed by an F-test to determine if the samples have equal variance. If the data did not fit a normal distribution, it was evaluated for pairwise comparisons using Wilcoxon Mann-Whitney U test. Correlation analysis was performed in SPSS using Pearson correlation. Analyses for gene-diet interactions was performed in SPSS as a univariate general linear model using a Type III sum-of-squares method.

Determination of protein glycation, oxidation and nitration adducts:

Targeted metabolomics was determined by stable isotopic dilution analysis liquid chromatography-tandem mass spectrometry (LC-MS/MS) by the protocol previously described (97). Analytes determined were: Nε-fructosyl-lysine (FL), Nε-carboxymethyl-lysine (CML), Nε-(1-carboxyethyl)lysine (CEL), methylglyoxal and 3-deoxyglucosone-derived hydroimidazolones (MG-H1 and 3DG-H, respectively), glucosepane, glutamic semialdehyde (GSA), 3-nitrotyrosine (3-NT), pentosidine, and related amino acids. Fasting plasma (10 μl) was diluted to 500 μl water and washed by diafiltration with 4-cycles of concentration to 50 μl and dilution to 500 μl with further aliquots of water. The resultant protein (50 μl) was delipidated by extraction 3 times with one-volume of water-saturated ether, the residual ether removed by centrifugal evaporation for 5 min under vacuum (20 mmHg) and the protein concentration determined by the Bradford method. An aliquot (100 μg protein) was then digested enzymatically by consecutive incubation with pepsin, pronase E and finally aminopeptidase with prolidase under argon over 4 days. Blanks and control digests of human serum albumin were performed concurrently to provide for protease autohydrolysis correction. Addition of thymol antioxidant and antibiotics after the neutralization step prevents artefactual oxidation and bacterial contamination. The process was performed aseptically and automatically by custom program in a CTC-PAL sample autoprocessor (CTC Analytics, Zwingen, Switzerland). Analytes were detected and quantified by stable isotopic dilution analysis electrospray positive ionization multiple reaction monitoring LC-MS/MS using an Acquity ultra high performance chromatography

(UPLC) system with a Xevo-TQS tandem mass spectrometer. Chromatography was with two graphitic Hypercarb™ columns (5 μm particle size; column-1, 2 × 50 mm and column-2, 2 × 250 mm) with eluent 0.1% trifluoroacetic acid in water with a custom program for multi-step gradient of acetonitrile and column switching.

Supplementary Material

Refer to Web version on PubMed Central for supplementary material.

Acknowledgements

We are grateful to Jennifer Cho and Jonathan Morrison for assistance with animal feeding, Barbara Nagel for histological and electron microscopy, Maria Stewart of Ingredion Inc. for dietary starches, Michael Freeman and Swati Biswas for Nrf2 +/− mice, Ryoji Nagai and Casper Schalkwijk for antibodies, and Jasper Weinberg for critical reading of the manuscript. Use of the EchoMRI-700 was supported by the Boston Nutrition Obesity Research Center (BNORC). Funding was supported by NIH RO1EY021212, RO1EY028559, and RO1EY026979 (to AT), USDA NIFA 2016–08885 (to AT and SR), USDA 8050-51000-089-01S (to AT), Thome Memorial Foundation (to AT), BrightFocus Foundation (to SR), the National Natural Science Foundation of China (NSFC) 81760177 (to SJ), and the Stanley N. Gershoff scholarship (to KMS). This material is based upon work supported by the U.S. Department of Agriculture – Agricultural Research Service (ARS), under Agreement No. 58-1950-4-003. The authors declare that they have no conflict of interest.

References

1. Owsley C, Clark ME, Huisingh CE, Curcio CA, and McGwin G Jr., Visual Function in Older Eyes in Normal Macular Health: Association with Incident Early Age-Related Macular Degeneration 3 Years Later. Invest Ophthalmol Vis Sci. 2016;57(4):1782–9. [PubMed: 27074381]
2. Age-Related Eye Disease Study 2 Research Group. Lutein + zeaxanthin and omega-3 fatty acids for age-related macular degeneration: the Age-Related Eye Disease Study 2 (AREDS2) randomized clinical trial. JAMA 2013;309:2005–15. [PubMed: 23644932]
3. Sobrin L, and Seddon JM. Nature and nurture- genes and environment- predict onset and progression of macular degeneration. Prog Retin Eye Res. 2014;40:1–15. [PubMed: 24374240]
4. Weikel KA, Chiu CJ, and Taylor A. Nutritional modulation of age-related macular degeneration. Molecular aspects of medicine. 2012;33(4):318–75. [PubMed: 22503690]
5. Chiu CJ, Milton RC, Klein R, Gensler G, and Taylor A. Dietary compound score and risk of age-related macular degeneration in the age-related eye disease study. Ophthalmology. 2009;116(5):939–46. [PubMed: 19410952]
6. Merle BMJ, Colijn JM, Cougnard-Gregoire A, de Koning-Backus APM, Delyfer MN, Kiefte-de Jong JC, et al. Mediterranean Diet and Incidence of Advanced Age-Related Macular Degeneration: The EYE-RISK Consortium. Ophthalmology. 2019;126(3):381–90. [PubMed: 30114418]
7. Chiu CJ, Chang ML, Zhang FF, Li T, Gensler G, Schleicher M, et al. The relationship of major American dietary patterns to age-related macular degeneration. American journal of ophthalmology. 2014;158(1):118–27 e1. [PubMed: 24792100]
8. Hogg RE, Woodside JV, McGrath A, Young IS, Vioque JL, Chakravarthy U, et al. Mediterranean Diet Score and Its Association with Age-Related Macular Degeneration: The European Eye Study. Ophthalmology. 2017;124(1):82–9. [PubMed: 27825655]
9. Kaushik S, Wang JJ, Flood V, Tan JS, Barclay AW, Wong TY, et al. Dietary glycemic index and the risk of age-related macular degeneration. Am J Clin Nutr. 2008;88(4):1104–10. [PubMed: 18842800]
10. de Koning-Backus APM, Buitendijk GHS, Kiefte-de Jong JC, Colijn JM, Hofman A, Vingerling JR, et al. Intake of Vegetables, Fruit, and Fish is Beneficial for Age-Related Macular Degeneration. American journal of ophthalmology. 2019;198:70–9. [PubMed: 30312575]

11. Chiu CJ, Klein R, Milton RC, Gensler G, and Taylor A. Does eating particular diets alter risk of age-related macular degeneration in users of the age-related eye disease study supplements? The British journal of ophthalmology. 2009:1241–6. [PubMed: 19508997]
12. Chong EW, Simpson JA, Robman LD, Hodge AM, Aung KZ, English DR, et al. Red meat and chicken consumption and its association with age-related macular degeneration. Am J Epidemiol. 2009;169(7):867–76. [PubMed: 19234096]
13. Chiu CJ, Milton RC, Klein R, Gensler G, and Taylor A. Dietary carbohydrate and the progression of age-related macular degeneration: a prospective study from the Age-Related Eye Disease Study. Am J Clin Nutr. 2007;86(4):1210–8. [PubMed: 17921404]
14. Chiu CJ, Hubbard LD, Armstrong J, Rogers G, Jacques PF, Chylack J, L. T, et al. Dietary glycemic index and carbohydrate in relation to early age-related macular degeneration. Am J Clin Nutr. 2006;83:880–6. [PubMed: 16600942]
15. Leung IY, Sandstrom MM, Zucker CL, Neuringer M, and Snodderly DM. Nutritional manipulation of primate retinas, II: effects of age, n-3 fatty acids, lutein, and zeaxanthin on retinal pigment epithelium. Invest Ophthalmol Vis Sci. 2004;45(9):3244–56. [PubMed: 15326147]
16. McGill TJ, Renner LM, and Neuringer M. Elevated Fundus Autofluorescence in Monkeys Deficient in Lutein, Zeaxanthin, and Omega-3 Fatty Acids. Invest Ophthalmol Vis Sci. 2016;57(3):1361–9. [PubMed: 27002296]
17. Weikel KA, Fitzgerald P, Shang F, Caceres MA, Bian Q, Handa JT, et al. Natural history of age-related retinal lesions that precede AMD in mice fed high or low glycemic index diets. Invest Ophthalmol Vis Sci. 2012;53(2):622–32. [PubMed: 22205601]
18. Rowan S, Jiang S, Korem T, Szymanski J, Chang ML, Szelog J, et al. Involvement of a gut-retina axis in protection against dietary glycemia-induced age-related macular degeneration. Proc Natl Acad Sci U S A. 2017;114(22):E4472–E81. [PubMed: 28507131]
19. Malek G, Johnson LV, Mace BE, Saloupis P, Schmechel DE, Rickman DW, et al. Apolipoprotein E allele-dependent pathogenesis: a model for age-related retinal degeneration. Proc Natl Acad Sci U S A. 2005;102(33):11900–5. [PubMed: 16079201]
20. Toomey CB, Kelly U, Saban DR, and Bowes Rickman C. Regulation of age-related macular degeneration-like pathology by complement factor H. Proc Natl Acad Sci U S A. 2015;112(23):E3040–9. [PubMed: 25991857]
21. Bonilha VL, Bell BA, Rayborn ME, Samuels IS, King A, Hollyfield JG, et al. Absence of DJ-1 causes age-related retinal abnormalities in association with increased oxidative stress. Free radical biology & medicine. 2017;104:226–37. [PubMed: 28088625]
22. Mitter SK, Song C, Qi X, Mao H, Rao H, Akin D, et al. Dysregulated autophagy in the RPE is associated with increased susceptibility to oxidative stress and AMD. Autophagy. 2014;10(11):1989–2005. [PubMed: 25484094]
23. Brown EE, DeWeerd AJ, Ildefonso CJ, Lewin AS, and Ash JD. Mitochondrial oxidative stress in the retinal pigment epithelium (RPE) led to metabolic dysfunction in both the RPE and retinal photoreceptors. Redox biology. 2019;24:101201.
24. Fujihara M, Bartels E, Nielsen LB, and Handa JT. A human apoB100 transgenic mouse expresses human apoB100 in the RPE and develops features of early AMD. Experimental eye research. 2009;88(6):1115–23. [PubMed: 19450445]
25. Uchiki T, Weikel KA, Jiao W, Shang F, Caceres A, Pawlak DB, et al. Glycation-altered proteolysis as a pathobiologic mechanism that links dietary glycemic index, aging, and age-related disease (in non diabetics). Aging Cell. 2012;11(1):1–13. [PubMed: 21967227]
26. Crabb JW, Miyagi M, Gu X, Shadrach K, West KA, Sakaguchi H, et al. Drusen proteome analysis: an approach to the etiology of age-related macular degeneration. Proc Natl Acad Sci U S A. 2002;99(23):14682–7. [PubMed: 12391305]
27. Handa JT, Verzijl N, Matsunaga H, Aotaki-Keen A, Lutty GA, te Koppele JM, et al. Increase in the advanced glycation end product pentosidine in Bruch's membrane with age. Invest Ophthalmol Vis Sci. 1999;40:775–9. [PubMed: 10067983]
28. Ishibashi T, Murata T, Hangai M, Nagai R, Horiuchi S, Lopez PF, et al. Advanced glycation end products in age-related macular degeneration. Archives of ophthalmology. 1998;116(12):1629–32. [PubMed: 9869793]

29. Howes KA, Liu Y, Dunaief JL, Milam A, Frederick JM, Marks A, et al. Receptor for advanced glycation end products and age-related macular degeneration. Invest Ophthalmol Vis Sci. 2004;45(10):3713–20. [PubMed: 15452081]
30. Ni J, Yuan X, Gu J, Yue X, Gu X, Nagaraj RH, et al. Plasma protein pentosidine and carboxymethyllysine, biomarkers for age-related macular degeneration. Mol Cell Proteomics. 2009;8(8):1921–33. [PubMed: 19435712]
31. Queisser MA, Yao D, Geisler S, Hammes HP, Lochnit G, Schleicher ED, et al. Hyperglycemia impairs proteasome function by methylglyoxal. Diabetes. 2010;59(3):670–8. [PubMed: 20009088]
32. Brown EE, Ball JD, Chen Z, Khurshid GS, Prosperi M, and Ash JD. The Common Antidiabetic Drug Metformin Reduces Odds of Developing Age-Related Macular Degeneration. Invest Ophthalmol Vis Sci. 2019;60(5):1470–7. [PubMed: 30973575]
33. Tonelli C, Chio IIC, and Tuveson DA. Transcriptional Regulation by Nrf2. Antioxid Redox Signal. 2018;29(17):1727–45. [PubMed: 28899199]
34. Xue M, Momiji H, Rabbani N, Barker G, Bretschneider T, Shmygol A, et al. Frequency Modulated Translocational Oscillations of Nrf2 Mediate the Antioxidant Response Element Cytoprotective Transcriptional Response. Antioxid Redox Signal. 2014.
35. Xue M, Rabbani N, Momiji H, Imbasi P, Anwar MM, Kitteringham N, et al. Transcriptional control of glyoxalase 1 by Nrf2 provides a stress-responsive defence against dicarbonyl glycation. The Biochemical journal. 2012;443(1):213–22. [PubMed: 22188542]
36. Brouwers O, Niessen PM, Ferreira I, Miyata T, Scheffer PG, Teerlink T, et al. Overexpression of glyoxalase-I reduces hyperglycemia-induced levels of advanced glycation end products and oxidative stress in diabetic rats. The Journal of biological chemistry. 2011;286(2):1374–80. [PubMed: 21056979]
37. Giacco F, Du X, D'Agati VD, Milne R, Sui G, Geoffrion M, et al. Knockdown of glyoxalase 1 mimics diabetic nephropathy in nondiabetic mice. Diabetes. 2014;63(1):291–9. [PubMed: 24062246]
38. Sanghvi VR, Leibold J, Mina M, Mohan P, Berishaj M, Li Z, et al. The Oncogenic Action of NRF2 Depends on De-glycation by Fructosamine-3-Kinase. Cell. 2019;178(4):807–19 e21. [PubMed: 31398338]
39. Pajares M, Jimenez-Moreno N, Garcia-Yague AJ, Escoll M, de Ceballos ML, Van Leuven F, et al. Transcription factor NFE2L2/NRF2 is a regulator of macroautophagy genes. Autophagy. 2016;12(10):1902–16. [PubMed: 27427974]
40. Holmstrom KM, Baird L, Zhang Y, Hargreaves I, Chalasani A, Land JM, et al. Nrf2 impacts cellular bioenergetics by controlling substrate availability for mitochondrial respiration. Biol Open. 2013;2(8):761–70. [PubMed: 23951401]
41. O'Mealey GB, Plafker KS, Berry WL, Janknecht R, Chan JY, and Plafker SM. A PGAM5-KEAP1-Nrf2 complex is required for stress-induced mitochondrial retrograde trafficking. Journal of cell science. 2017;130(20):3467–80. [PubMed: 28839075]
42. Piantadosi CA, Carraway MS, Babiker A, and Suliman HB. Heme oxygenase-1 regulates cardiac mitochondrial biogenesis via Nrf2-mediated transcriptional control of nuclear respiratory factor-1. Circulation research. 2008;103(11):1232–40. [PubMed: 18845810]
43. Gureev AP, Shaforostova EA, and Popov VN. Regulation of Mitochondrial Biogenesis as a Way for Active Longevity: Interaction Between the Nrf2 and PGC-1alpha Signaling Pathways. Front Genet. 2019;10:435. [PubMed: 31139208]
44. Ramos-Gomez M, Kwak MK, Dolan PM, Itoh K, Yamamoto M, Talalay P, et al. Sensitivity to carcinogenesis is increased and chemoprotective efficacy of enzyme inducers is lost in nrf2 transcription factor-deficient mice. Proc Natl Acad Sci U S A. 2001;98(6):3410–5. [PubMed: 11248092]
45. Beyer TA, Xu W, Teupser D, auf dem Keller U, Bugnon P, Hildt E, et al. Impaired liver regeneration in Nrf2 knockout mice: role of ROS-mediated insulin/IGF-1 resistance. EMBO J. 2008;27(1):212–23. [PubMed: 18059474]
46. Cho HY, Jedlicka AE, Reddy SP, Kensler TW, Yamamoto M, Zhang LY, et al. Role of NRF2 in protection against hyperoxic lung injury in mice. Am J Respir Cell Mol Biol. 2002;26(2):175–82. [PubMed: 11804867]

47. Hubbs AF, Benkovic SA, Miller DB, O'Callaghan JP, Battelli L, Schwegler-Berry D, et al. Vacuolar leukoencephalopathy with widespread astrogliosis in mice lacking transcription factor Nrf2. Am J Pathol. 2007;170(6):2068–76. [PubMed: 17525273]
48. Kansanen E, Kuosmanen SM, Leinonen H, and Levonen AL. The Keap1-Nrf2 pathway: Mechanisms of activation and dysregulation in cancer. Redox biology. 2013;1(1):45–9. [PubMed: 24024136]
49. Wei Y, Gong J, Yoshida T, Eberhart CG, Xu Z, Kombairaju P, et al. Nrf2 has a protective role against neuronal and capillary degeneration in retinal ischemia-reperfusion injury. Free radical biology & medicine. 2011;51(1):216–24. [PubMed: 21545836]
50. Zhao Z, Chen Y, Wang J, Sternberg P, Freeman ML, Grossniklaus HE, et al. Age-Related Retinopathy in NRF2-Deficient Mice. PloS one. 2011;6(4):e19456-.
51. Zhao Z, Xu P, Jie Z, Zuo Y, Yu B, Soong L, et al. gammadelta T cells as a major source of IL-17 production during age-dependent RPE degeneration. Invest Ophthalmol Vis Sci. 2014;55(10):6580–9. [PubMed: 25212781]
52. Felszeghy S, Viiri J, Paterno JJ, Hyttinen JMT, Koskela A, Chen M, et al. Loss of NRF-2 and PGC-1alpha genes leads to retinal pigment epithelium damage resembling dry age-related macular degeneration. Redox biology. 2019;20:1–12. [PubMed: 30253279]
53. Xiong W, MacColl Garfinkel AE, Li Y, Benowitz LI, and Cepko CL. NRF2 promotes neuronal survival in neurodegeneration and acute nerve damage. The Journal of clinical investigation. 2015;125(4):1433–45. [PubMed: 25798616]
54. Wang J, Zhao J, Cui X, Mysona BA, Navneet S, Saul A, et al. The molecular chaperone sigma 1 receptor mediates rescue of retinal cone photoreceptor cells via modulation of NRF2. Free radical biology & medicine. 2019;134:604–16. [PubMed: 30743048]
55. Ebrahimi KB, Cano M, Rhee J, Datta S, Wang L, and Handa JT. Oxidative Stress Induces an Interactive Decline in Wnt and Nrf2 Signaling in Degenerating Retinal Pigment Epithelium. Antioxid Redox Signal. 2018;29(4):389–407. [PubMed: 29186981]
56. Sachdeva MM, Cano M, and Handa JT. Nrf2 signaling is impaired in the aging RPE given an oxidative insult. Experimental eye research. 2014;119:111–4. [PubMed: 24216314]
57. Lambros ML, and Plafker SM. Oxidative Stress and the Nrf2 Anti-Oxidant Transcription Factor in Age-Related Macular Degeneration. Adv Exp Med Biol. 2016;854:67–72. [PubMed: 26427395]
58. Pawlak DB, Kushner JA, and Ludwig DS. Effects of dietary glycaemic index on adiposity, glucose homoeostasis, and plasma lipids in animals. Lancet. 2004;364(9436):778–85. [PubMed: 15337404]
59. Isken F, Klaus S, Petzke KJ, Loddenkemper C, Pfeiffer AF, and Weickert MO. Impairment of fat oxidation under high vs low glycemic index diet occurs prior to the development of an obese phenotype. Am J Physiol Endocrinol Metab. 2010;298(2):E297–95.
60. Pi JB, Leung L, Xue P, Wang WP, Hou YY, Liu DX, et al. Deficiency in the Nuclear Factor E2-related Factor-2 Transcription Factor Results in Impaired Adipogenesis and Protects against Diet-induced Obesity. Journal of Biological Chemistry. 2010;285(12):9292–300.
61. Zanzottera EC, Messinger JD, Ach T, Smith RT, Freund KB, and Curcio CA. The Project MACULA Retinal Pigment Epithelium Grading System for Histology and Optical Coherence Tomography in Age-Related Macular Degeneration. Invest Ophthalmol Vis Sci. 2015;56(5):3253–68. [PubMed: 25813989]
62. Sarks JP, Sarks SH, and Killingsworth MC. Evolution of geographic atrophy of the retinal pigment epithelium. Eye (London, England). 1988;2 (Pt 5):552–77.
63. Bhutto I, and Lutty G. Understanding age-related macular degeneration (AMD): relationships between the photoreceptor/retinal pigment epithelium/Bruch's membrane/choriocapillaris complex. Molecular aspects of medicine. 2012;33(4):295–317. [PubMed: 22542780]
64. Rowan S, Weikel K, Chang ML, Nagel BA, Thinschmidt JS, Carey A, et al. Cfh genotype interacts with dietary glycemic index to modulate age-related macular degeneration-like features in mice. Invest Ophthalmol Vis Sci. 2014;55(1):492–501. [PubMed: 24370827]
65. Killingsworth MC, Sarks JP, and Sarks SH. Macrophages related to Bruch's membrane in age-related macular degeneration. Eye (London, England). 1990;4 (Pt 4):613–21.

66. Cherepanoff S, McMenamin P, Gillies MC, Kettle E, and Sarks SH. Bruch's membrane and choroidal macrophages in early and advanced age-related macular degeneration. The British journal of ophthalmology. 2010;94(7):918–25. [PubMed: 19965817]

67. Landowski M, Kelly U, Klingeborn M, Groelle M, Ding JD, Grigsby D, et al. Human complement factor H Y402H polymorphism causes an age-related macular degeneration phenotype and lipoprotein dysregulation in mice. Proc Natl Acad Sci U S A. 2019;116(9):3703–11. [PubMed: 30808757]

68. Ufret-Vincenty RL, Aredo B, Liu X, McMahon A, Chen PW, Sun H, et al. Transgenic mice expressing variants of complement factor H develop AMD-like retinal findings. Invest Ophthalmol Vis Sci. 2010;51(11):5878–87. [PubMed: 20538999]

69. Espinosa-Heidmann DG, Sall J, Hernandez EP, and Cousins SW. Basal laminar deposit formation in APO B100 transgenic mice: complex interactions between dietary fat, blue light, and vitamin E. Invest Ophthalmol Vis Sci. 2004;45(1):260–6. [PubMed: 14691182]

70. Zhang M, Chu Y, Mowery J, Konkel B, Galli S, Theos AC, et al. Pgc-1alpha repression and high-fat diet induce age-related macular degeneration-like phenotypes in mice. Dis Model Mech. 2018;11(9).

71. Choi W, Moult EM, Waheed NK, Adhi M, Lee B, Lu CD, et al. Ultrahigh-Speed, Swept-Source Optical Coherence Tomography Angiography in Nonexudative Age-Related Macular Degeneration with Geographic Atrophy. Ophthalmology. 2015;122(12):2532–44. [PubMed: 26481819]

72. Sohn EH, Flamme-Wiese MJ, Whitmore SS, Workalemahu G, Marneros AG, Boese EA, et al. Choriocapillaris Degeneration in Geographic Atrophy. Am J Pathol. 2019;189(7):1473–80. [PubMed: 31051169]

73. Terluk MR, Kapphahn RJ, Soukup LM, Gong H, Gallardo C, Montezuma SR, et al. Investigating mitochondria as a target for treating age-related macular degeneration. The Journal of neuroscience : the official journal of the Society for Neuroscience. 2015;35(18):7304–11. [PubMed: 25948278]

74. Kenney MC, Atilano SR, Boyer D, Chwa M, Chak G, Chinichian S, et al. Characterization of retinal and blood mitochondrial DNA from age-related macular degeneration patients. Invest Ophthalmol Vis Sci. 2010;51(8):4289–97. [PubMed: 20357205]

75. Feher J, Kovacs I, Artico M, Cavallotti C, Papale A, and Balacco Gabrieli C. Mitochondrial alterations of retinal pigment epithelium in age-related macular degeneration. Neurobiol Aging. 2006;27(7):983–93. [PubMed: 15979212]

76. Ferrington DA, Ebeling MC, Kapphahn RJ, Terluk MR, Fisher CR, Polanco JR, et al. Altered bioenergetics and enhanced resistance to oxidative stress in human retinal pigment epithelial cells from donors with age-related macular degeneration. Redox biology. 2017;13:255–65. [PubMed: 28600982]

77. Satish S, Philipose H, Rosales MAB, and Saint-Geniez M. Pharmaceutical Induction of PGC-1alpha Promotes Retinal Pigment Epithelial Cell Metabolism and Protects against Oxidative Damage. Oxidative medicine and cellular longevity. 2018;2018:9248640.

78. Takahashi A, Takabatake Y, Kimura T, Maejima I, Namba T, Yamamoto T, et al. Autophagy Inhibits the Accumulation of Advanced Glycation End Products by Promoting Lysosomal Biogenesis and Function in the Kidney Proximal Tubules. Diabetes. 2017.

79. Zhang Y, Cross SD, Stanton JB, Marmorstein AD, Le YZ, and Marmorstein LY. Early AMD-like defects in the RPE and retinal degeneration in aged mice with RPE-specific deletion of Atg5 or Atg7. Molecular vision. 2017;23:228–41. [PubMed: 28465655]

80. Rowan S, Bejarano E, and Taylor A. Mechanistic targeting of advanced glycation end-products in age-related diseases. Biochim Biophys Acta Mol Basis Dis. 2018;1864(12):3631–43. [PubMed: 30279139]

81. Hayes JD, and Dinkova-Kostova AT. The Nrf2 regulatory network provides an interface between redox and intermediary metabolism. Trends Biochem Sci. 2014;39(4):199–218. [PubMed: 24647116]

82. Kanow MA, Giarmarco MM, Jankowski CS, Tsantilas K, Engel AL, Du J, et al. Biochemical adaptations of the retina and retinal pigment epithelium support a metabolic ecosystem in the vertebrate eye. Elife. 2017;6.

83. Huang J, Gu S, Chen M, Zhang SJ, Jiang Z, Chen X, et al. Abnormal mTORC1 signaling leads to retinal pigment epithelium degeneration. Theranostics. 2019;9(4):1170–80. [PubMed: 30867823]
84. Xu L, Kong L, Wang J, and Ash JD. Stimulation of AMPK prevents degeneration of photoreceptors and the retinal pigment epithelium. Proc Natl Acad Sci U S A. 2018;115(41):10475–80. [PubMed: 30249643]
85. Blander JM, Longman RS, Iliev ID, Sonnenberg GF, and Artis D. Regulation of inflammation by microbiota interactions with the host. Nature immunology. 2017;18(8):851–60. [PubMed: 28722709]
86. Ardeljan CP, Ardeljan D, Abu-Asab M, and Chan CC. Inflammation and Cell Death in Age-Related Macular Degeneration: An Immunopathological and Ultrastructural Model. J Clin Med. 2014;3(4):1542–60. [PubMed: 25580276]
87. Hollyfield JG, Bonilha VL, Rayborn ME, Yang X, Shadrach KG, Lu L, et al. Oxidative damage-induced inflammation initiates age-related macular degeneration. Nature medicine. 2008;14(2):194–8.
88. Doyle SL, Campbell M, Ozaki E, Salomon RG, Mori A, Kenna PF, et al. NLRP3 has a protective role in age-related macular degeneration through the induction of IL-18 by drusen components. Nature medicine. 2012;18(5):791–8.
89. Zinkernagel MS, Zysset-Burri DC, Keller I, Berger LE, Leichtle AB, Largiader CR, et al. Association of the Intestinal Microbiome with the Development of Neovascular Age-Related Macular Degeneration. Sci Rep. 2017;7:40826. [PubMed: 28094305]
90. Akiyama K, Warabi E, Okada K, Yanagawa T, Ishii T, Kose K, et al. Deletion of both p62 and Nrf2 spontaneously results in the development of nonalcoholic steatohepatitis. Exp Anim. 2018;67(2):201–18. [PubMed: 29276215]
91. Thaiss CA, Levy M, Grosheva I, Zheng D, Soffer E, Blacher E, et al. Hyperglycemia drives intestinal barrier dysfunction and risk for enteric infection. Science. 2018;359(6382):1376–83. [PubMed: 29519916]
92. Singh R, Chandrashekharappa S, Bodduluri SR, Baby BV, Hegde B, Kotla NG, et al. Enhancement of the gut barrier integrity by a microbial metabolite through the Nrf2 pathway. Nat Commun. 2019;10(1):89. [PubMed: 30626868]
93. He C, Huang L, Lei P, Liu X, Li B, and Shan Y. Sulforaphane Normalizes Intestinal Flora and Enhances Gut Barrier in Mice with BBN-Induced Bladder Cancer. Mol Nutr Food Res. 2018;62(24):e1800427.
94. Axelsson AS, Tubbs E, Mecham B, Chacko S, Nenonen HA, Tang Y, et al. Sulforaphane reduces hepatic glucose production and improves glucose control in patients with type 2 diabetes. Science translational medicine. 2017;9(394).
95. Aleksunes LM, Reisman SA, Yeager RL, Goedken MJ, and Klaassen CD. Nuclear factor erythroid 2-related factor 2 deletion impairs glucose tolerance and exacerbates hyperglycemia in type 1 diabetic mice. J Pharmacol Exp Ther. 2010;333(1):140–51. [PubMed: 20086057]
96. Scribner KB, Pawlak DB, and Ludwig DS. Hepatic steatosis and increased adiposity in mice consuming rapidly vs. slowly absorbed carbohydrate. Obesity (Silver Spring). 2007;15(9):2190–9. [PubMed: 17890486]
97. Rabbani N, Shaheen F, Anwar A, Masania J, and Thornalley PJ. Assay of methylglyoxal-derived protein and nucleotide AGEs. BiochemSocTrans. 2014;42(2):511–7.

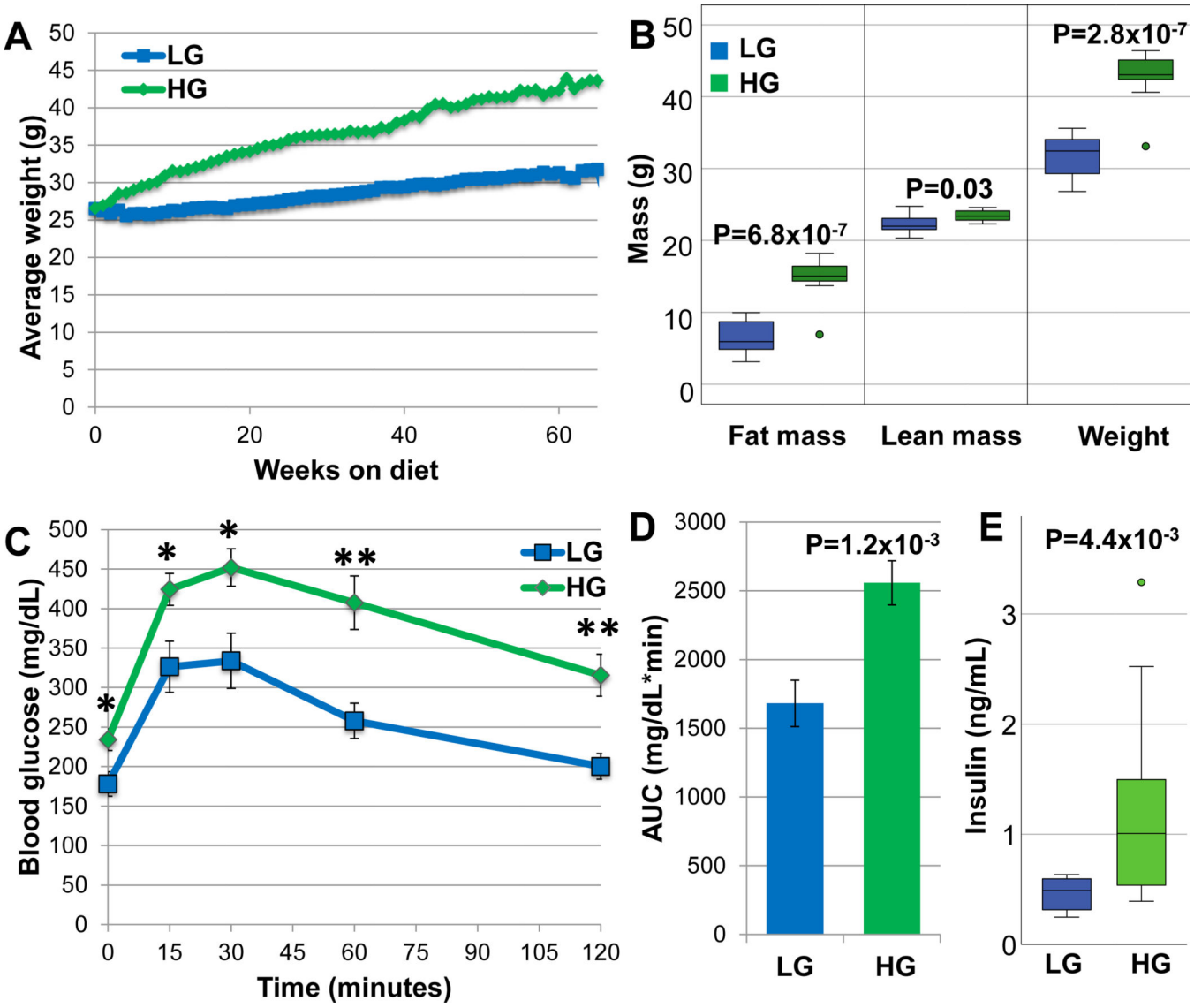

Figure 1.

Nrf2-HG mice develop obesity, hyperglycemia, and glucose intolerance. (**A**) The average body weight of Nrf2-HG mice increased 35% over Nrf2-LG mice with aging. (**B**) Body mass composition at 13-mo. indicates that the increased body weight was from increased fat mass and not lean body mass. (**C**) Intraperitoneal glucose tolerance tests at 10-mo. indicate that Nrf2-HG mice have significantly increased fasting blood glucose and impaired glucose tolerance relative to Nrf2-LG mice. (**D**) Quantitation of the area under the curve for the glucose tolerance test indicates 52% increased AUC for Nrf2-HG mice. (**E**) Fasting insulin levels at 18-mo. were increased 148% in Nrf2-HG mice. Data points indicate means and error bars indicate SEM. All statistical tests performed were Student's T-tests: *, P<0.05; **, P<0.01. Sample size is n=20 (HG), n=19 (LG) in (**A**); n=10 (HG), n=12 (LG) in (**B**); n=11 in (**C,D**); n=14 in (**E**)

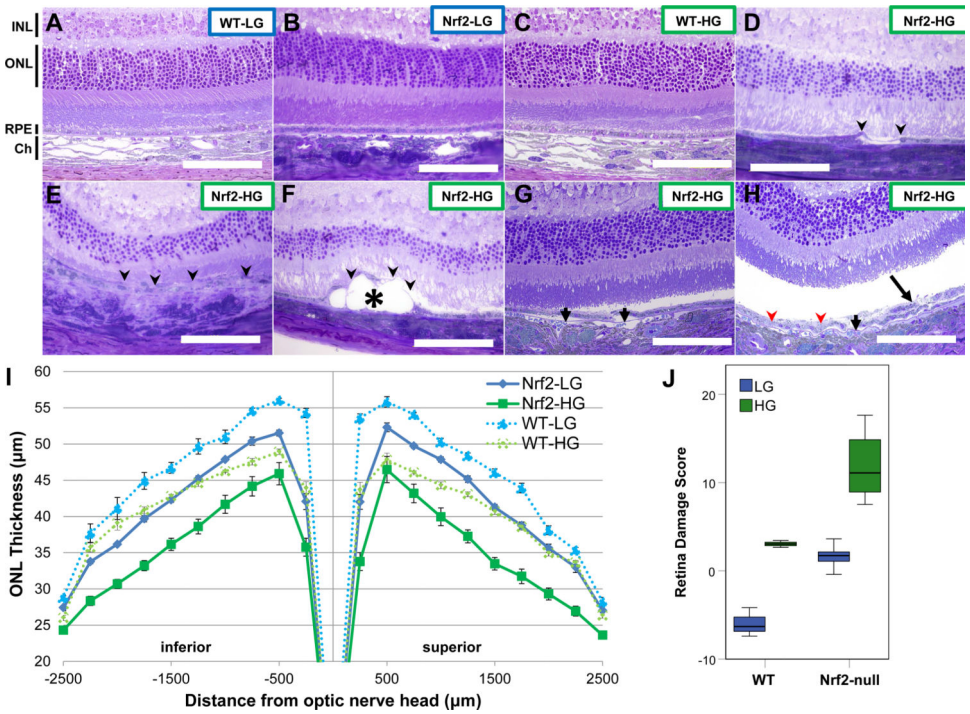

Figure 2.

Nrf2-HG mice develop features of atrophic age-related macular degeneration. (**A-H**) Toluidine blue stained sections through the retinas of WT-LG (**A**), Nrf2-LG (**B**), and WT-HG (**C**), have normal architecture: INL layers from neural cells, ONL layers from photoreceptors, the RPE, and the choroid are all clearly observed. In contrast, Nrf2-HG mouse retinas (**D-H**) show multiple lesions including: RPE atrophy (arrowheads), deposits (asterisk), RPE detachments from Bruch's membrane (short arrows), hypopigmentation (red arrowheads), and multilayered/dysmorphic RPE (long arrow). Higher magnification images of Figures 2A–H are shown in Supplementary Figure 1. (**I**) Measurement of ONL thickness across the retinas of each dietary and genotype group indicates moderate thinning of WT-HG and Nrf2-LG ONL, but severe thinning of Nrf2-HG ONL relative to WT-LG ONL. (**J**) Boxplots of retina damage score, based on the area under the ONL thickness plot, show increased retina damage score in Nrf2-HG mice compared to all other groups. Abbreviations: Ch-choroid, INL-inner nuclear layer, ONL –outer nuclear layer, RPE –retinal pigmented epithelium. Data points in (**I**) indicate means and error bars indicate SEM. Sample size is n=10 (Nrf2-HG), n=11 (Nrf2-LG), n=3 (WT) in (**I,J**). Scale bar is 100µm.

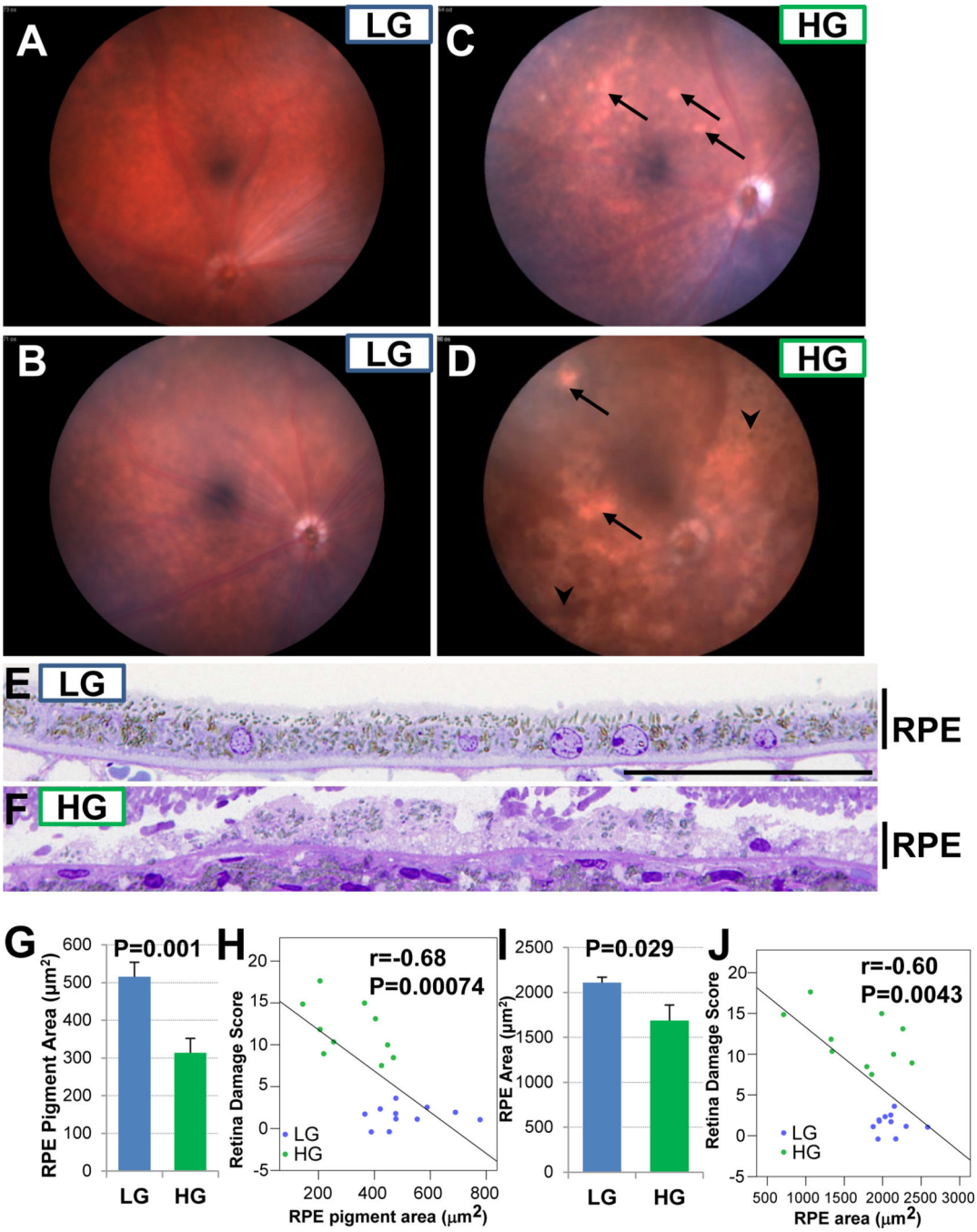

Figure 3.

Nrf2-HG eyes develop pigment abnormalities and RPE thinning. (**A-D**) Fundus photographs show areas of hypopigmentation (arrows) and hyperpigmentation (arrowheads) in Nrf2-HG eyes. (**E-F**) Toluidine blue stained high magnification sections through the RPE show hypopigmentation and thinning of the Nrf2-HG RPE. (**G-H**) Quantitation of pigment granule area demonstrates hypopigmentation in Nrf2-HG RPE (**G**) that is negatively correlated with the retina damage score (**H**). (**I-J**) Quantitation of RPE area demonstrates thinning of the Nrf2-HG RPE (**I**) that is negatively correlated with the retina damage score

(**J**). Bar graphs indicate means and error bars indicate SEM. Statistical tests performed were Student's T-test (**G,I**) or Pearson correlation (**H,J**). Sample size is n=10 (Nrf2-HG), n=11 (Nrf2-LG) in (**G-J**). Scale bar in (**E**) is 50 μm.

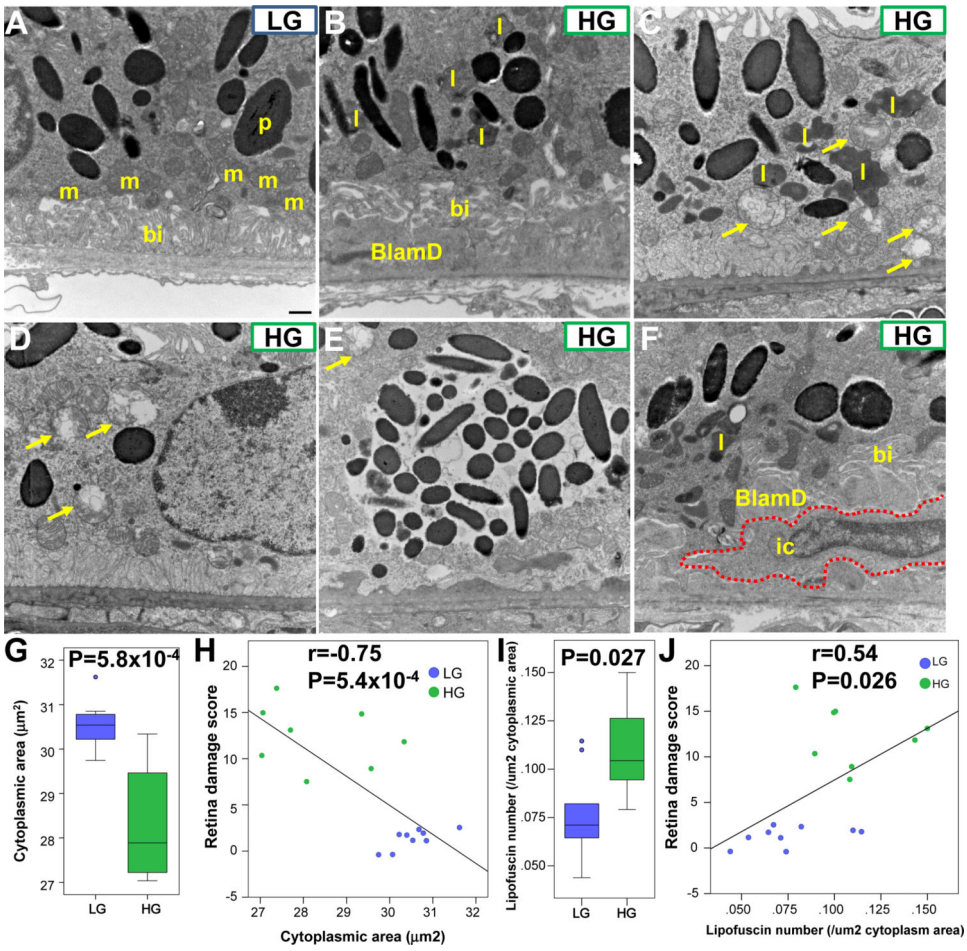

Figure 4.

Ultrastructural changes, mitochondrial degeneration, and lipofuscin accumulation in Nrf2-HG RPE. (**A-F**) Electron micrographs of RPE cells showing intact basal infoldings, mitochondria, and spindle-shaped pigment granule cells in Nrf2-LG RPE (**A**), whereas Nrf2-HG RPE have missing or mislocalized basal infoldings (**B**), accumulation of lipofuscin (**B, C, F**), accumulation of basal laminar deposits (**B, F**), swollen and degenerated mitochondria (arrows, **C-E**), hypopigmentation (**D**), hyperpigmentation (**E**), and infiltrating cells (red dashed line, **F**). (**G-H**) Boxplots indicate that Nrf2-HG RPE has reduced cytoplasmic area (**G**), which is negatively correlated with retina damage score (**H**). (**I-J**) Boxplots indicate that Nrf2-HG has increased numbers of lipofuscin granules (**I**), which are positively correlated with retina damage score (**J**). Abbreviations: bi-basal infoldings, BlamD-basal laminar deposits, ic-infiltrating cell, l-lipofuscin granule, m-mitochondria, p-pigment granule. Statistical tests performed were Student's T-test (**G,I**) or Pearson correlation (**H,J**). Sample size is n=8 (Nrf2-HG), n=9 (Nrf2-LG). Scale bar in (**A**) is 500 nm.

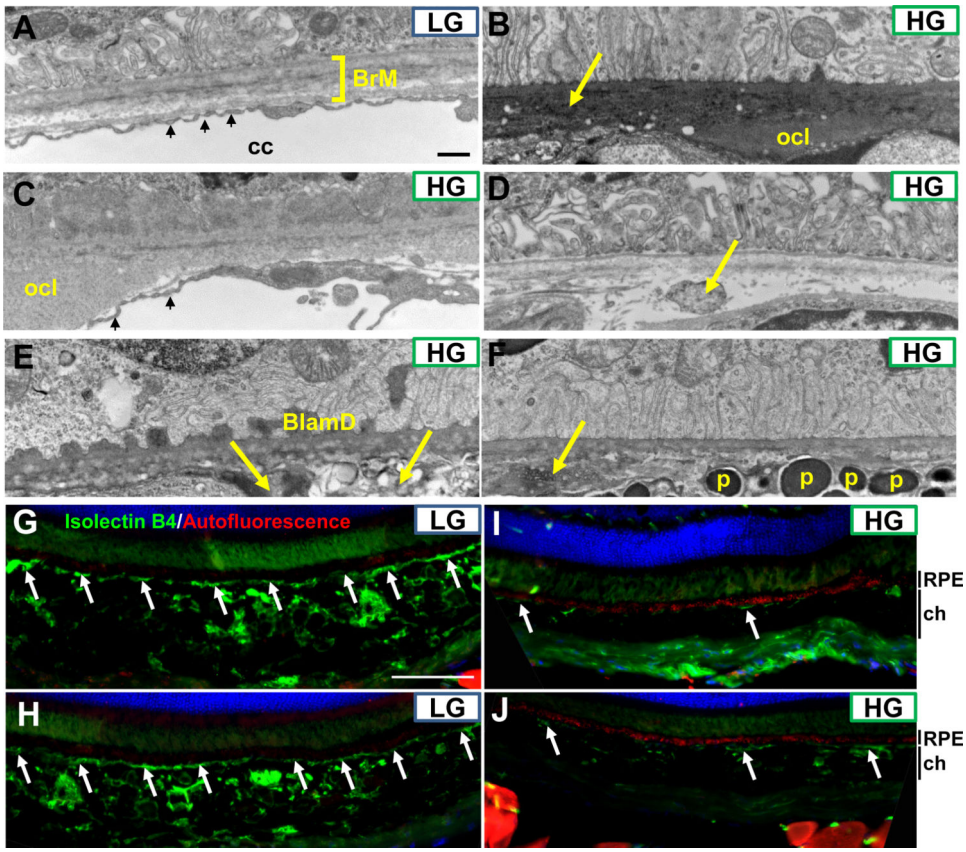

Figure 5.

Sub-RPE deposits, Bruch's membrane abnormalities, and loss of choriocapillaris in Nrf2-HG eyes. (**A-F**) Electron micrographs of the basal RPE, Bruch's membrane, and choriocapillaris indicate the lack of sub-RPE deposits, intact penta-laminar Bruch's membrane structure (square bracket in **A**), and well-fenestrated choriocapillaris (small arrows in **A**) in Nrf2-LG eyes (**A**). Nrf2-HG eyes contain multiple sub-RPE deposits, including outer collagenous layer deposits (**B,C**), basal laminar deposits (**E**), and other heterogeneous deposits/debris (arrows in **B, D, E, F**). The choriocapillaris was largely absent except in a few areas (small arrows, **C**) and choroidal tissue, including melanocytes containing pigmented granules, were localized proximal to Bruch's membrane (**F**). (**G-J**) Immunofluorescent staining for blood vessels via IsolectinB4 staining (green) or for autofluorescence (red) indicate intact choriocapillaris (arrows) and choroidal blood vessels in Nrf2-LG eyes (**G,H**) that are absent or degenerated in Nrf2-HG eyes (**I,J**), whereas autofluorescent puncta are highly increased in Nrf2-HG RPE (red staining in **I,J**). Abbreviations: BlamD-basal laminar deposit, BrM-Bruch's membrane, cc-choriocapillaris, ch-choroid, ocl-outer collagenous layer deposit, p-pigment granule within melanocyte. Scale bar in (**A**) is 500nm; in (**G**) is 100 μm.

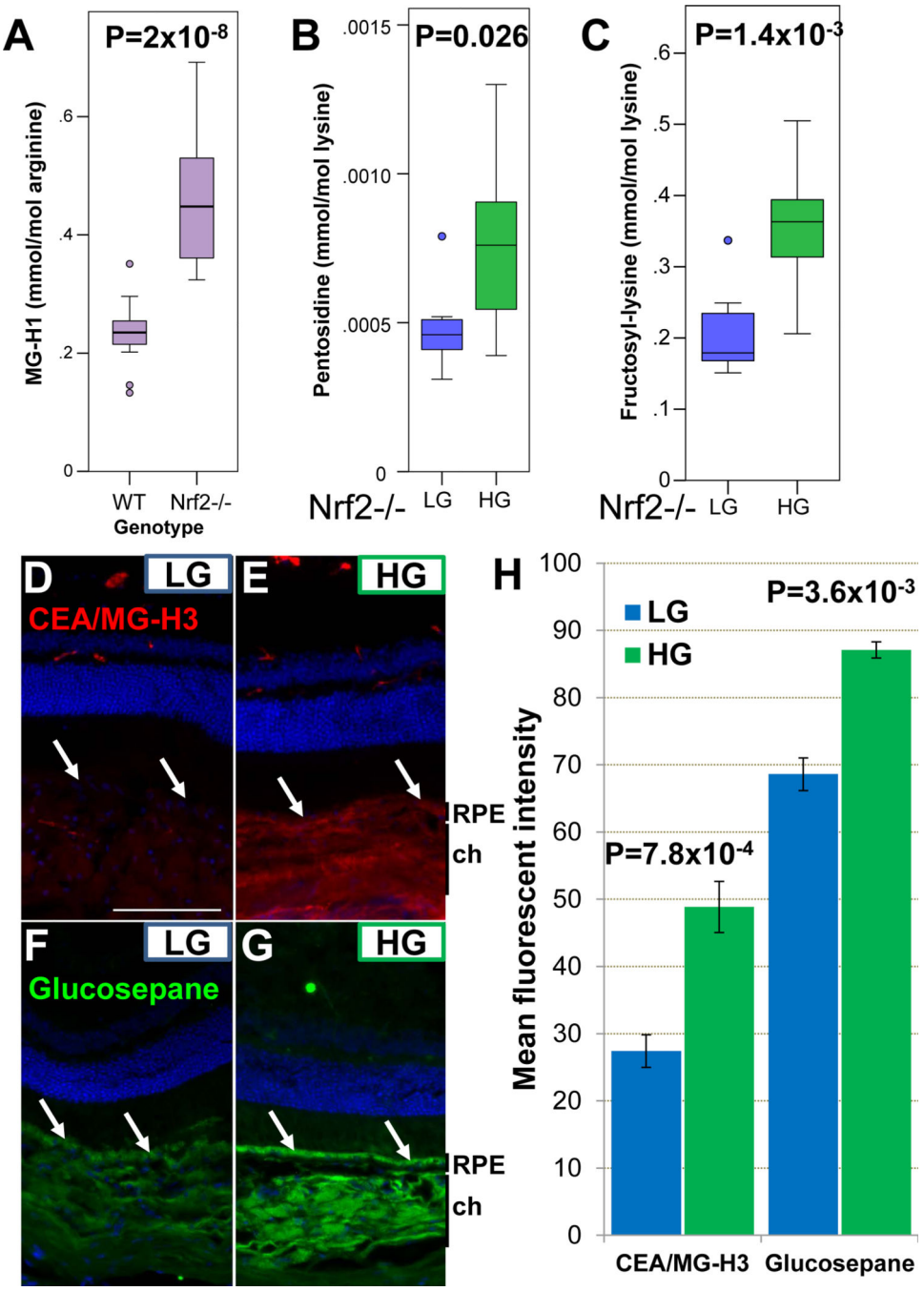

Figure 6.

Accumulation of AGEs in the plasma and RPE of Nrf2-HG mice. (**A**) Plasma levels of MG-H1 are increased in the plasma of 18-mo. Nrf2-null mice relative to 24 mo. WT mice. (**B-C**) Plasma pentosidine and fructosyl-lysine are increased in the plasma of Nrf2-HG mice. (**D-G**) Immunofluorescent detection of CEA (red, **D,E**) and glucosepane (green, **F,G**) shows increased AGE levels in the RPE (arrows) and choroid in Nrf2-HG eyes. CEA is the more stable hydrolysis product of MG-H3. (**H**) Quantitation of fluorescent staining indicates statistically significant increases in CEA and glucosepane in the RPE of Nrf2-HG mice.

Statistical tests performed were Student's T-test. Bars indicate mean and errors bars indicate SEM. Sample size is n=16 (**A**), n=8 (**B-C**), n=4 (**H**). Abbreviations: ch-choroid, rpe-retinal pigmented epithelium. Scale bar in (**D**) is 100 μm.

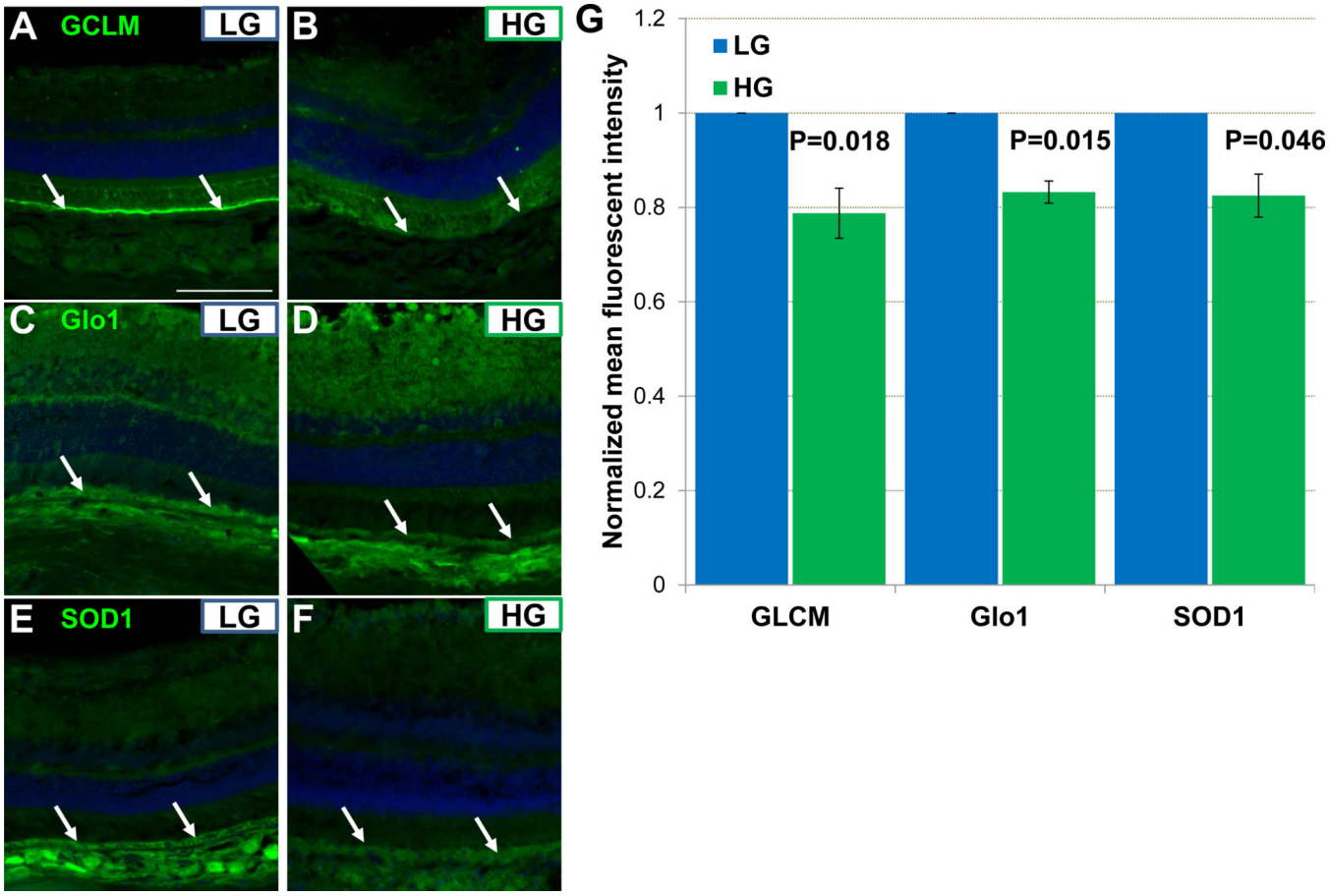

Figure 7.

Increased antioxidant and antiglycative potential of Nrf2-LG RPE. (**A**-**F**) Immunofluorescent detection of GLCM (A,B), Glo1 (C,D), or SOD1 (E,F) show increased staining in Nrf2-LG RPE (arrows). (G) Quantitation of fluorescent staining indicates statistically significant but modest relative increases in GCLM, Glo1, and SOD1 in Nrf2-LG RPE. Statistical tests performed were Student's T-test. Bars indicate mean and error bars indicate SEM. Sample size is n=4. Scale bar in (**A**) is 100 μm.